BIFURCATION AND CHAOS IN YAW MOTION OF A SHIP AT LOWER SPEED IN WAVES AND ITS PREVENTION USING OPTIMAL CONTROL

Atsuo Maki, Osaka University atsuo@maritime.kobe-u.ac.jp
Umeda Naoya, Osaka University umeda@naoe.eng.osaka-u.ac.jp

ABSTRACT

In this work, the authors investigated a low-speed broaching-to phenomenon of a ship in stern quartering waves with nonlinear dynamics using a surge-sway-yaw-roll simulation model. As a result, a standard bifurcation technique of periodic orbits confirmed the occurrence of the phenomenon as a flip bifurcation, which had been identified in the previous works. The calculation of Lyapunov exponents demonstrates that this phenomenon could result in chaos via a Feigenbaum cascade. The experimental record of this phenomenon is also presented with a physical model of the ONR tumblehome. Further, to prevent this phenomenon, an optimal control theory is applied. Here the optimal control law was numerically obtained by a nonlinear programming technique for minimising the performance index, which is defined as the variance of yaw angle. The obtained control successfully prevents the occurrence of yaw instability. This suggests, if this conclusion is widely applicable for ships, that this low-speed broaching could be avoided by appropriate operation so that it could be noted in physics-based operational guidance but it does not have to be included in a design criterion.

Keywords: *subharmonic yaw motion, chaos, flip bifurcation, maximum Lyapunov exponents and optimal control theory*

1. INTRODUCTION

At the IMO, new-generation intact stability criteria are now under development for three major capsizing scenarios (Japan et al., 2007). Manoeuvring-related problem such as broaching-to is one of these problems. So far, broaching-to associated with surf-riding has been investigated from various aspects (e.g. Motora et al., 1982). This phenomenon occurs when a ship runs with relatively high-speed, e.g. the Froude number of 0.3 or over in following and quartering seas, and it was well confirmed that it could result in capsizing of even a ship complying with the current prescriptive criteria. On the other hand, it was mentioned in literature (Oakley et al., 1974) that another type of broaching could occur at lower speed. Here a ship is overtaken by waves but her oscillatory yaw motion could

drastically develop. Kan (1990) observed a period-doubling bifurcation of roll and yaw in his free-running model experiments. Spyrou (1996, 1997) reproduced this phenomenon using numerical simulations and explained it as a sequence of flip and fold bifurcations. This phenomenon also can be interpreted as parametric resonance or Mathieu type instability in yaw in Nomoto's KT manoeuvring model with wave-induced yaw moment. It was also shown in the above references that this type of broaching can be avoided by increasing differential control gain. Since broaching can be regarded as inability of course-keeping despite the application of maximum steering effort, whether optimal control can exclude yaw instability or not is one of crucial questions for regulators and operators. Recently the authors also observed such yaw instability in their free-running model

experiments during an attempt for simulating optimal control in waves. Then, to supplement existing numerical simulation for further understanding this phenomenon, stability of periodic orbits is systematically investigated. Further we attempted to more directly obtain an answer to the question that the maximum steering effort can exclude yaw instability in light of optimal control theory with a proposed performance index.

2. FREE RUNNING MODEL EXPERIMENT

As mentioned above, experimental result about subharmonic yaw motion was reported by Kan (1990). At that time he used a container ship model, then he measured yaw instability and capsizing caused by this phenomenon. On the other hand, we also measured yaw instability in a seakeeping and manoeuvring basin of NRIFE (National Research Institute of Fisheries Engineering), with the ONR (Office of Naval Research) tumblehome vessel. Her principal particulars, body plan and photo are shown in Table 1, Fig.1 and Fig.2, respectively.

Table 1. Principal particulars of the ONR tumblehome vessel.

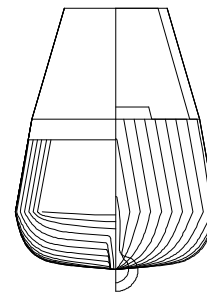| Items	Ship
Length : L	154.0 m
Breadth : B	18.78 m
Depth : D	14.50 m
Draught : d	5.494 m
Block coefficient : C_b	0.5354
Metacentric hight : GM	2.068 m
L.C.B. (aft)	2.587 m
Rudder Area Ratio	1/14.77
Radius of gyration in pitch: K_{yy}/L	0.246

Figure 1.Body plan of the ONR tumblehome vessel.

Figure 2. Photo of the used model ship.

This is a good example of a high-speed slender vessel, and has its comprehensive data in the public domain. Her above-water hull has tumblehome and a wave-piercing bow. The ship is equipped with twin screws and twin rudders. The details of the experiments were reported by Umeda et al. (2008A).
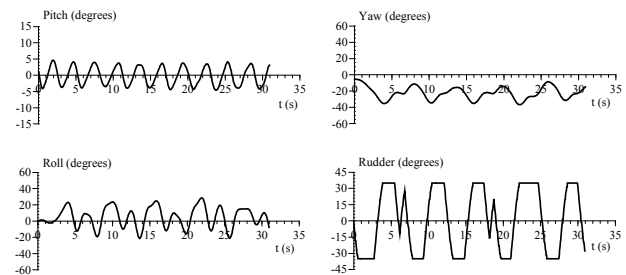

Figure 3. Time history of sub-harmonic motion obtained from experiment with $H/\lambda = 0.05$, $\lambda/L = 1.25$ and the auto pilot course of -22.5 degrees with $Fn = 0.3$.

Here the ship model initially drifted near the wave maker and then the propellers and the autopilot control were activated. The propeller revolutions were set to attempt to control the specified nominal Froude numbers during the model runs and a proportional autopilot with the rudder gain of 100.0 was used. The reason why we used such large rudder gain is to roughly simulate a Bang-Bang rudder control.

Fig.3 and Fig.4 indicate the time histories of ship motion as an example of yaw instability. However this Bang-Bang-typed but non-optimal control itself has strong nonlinearity so that it could lead to this phenomenon.
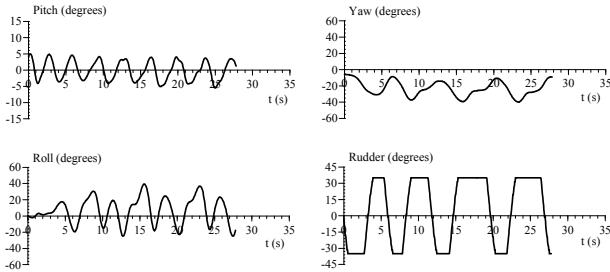

Figure 4. Time history of sub-harmonic motion obtained from experiment with $H/\lambda = 0.05$, $\lambda/L = 1.25$ and the auto pilot course of -22.5 degrees with $Fn = 0.35$.
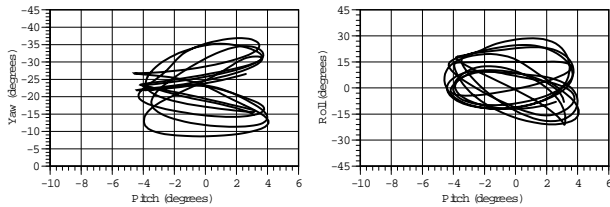

Figure 5. Phase trajectories of sub-harmonic motion obtained from experiment with $H/\lambda = 0.05$, $\lambda/L = 1.25$ and the auto pilot course of -22.5 degrees with $Fn = 0.3$.
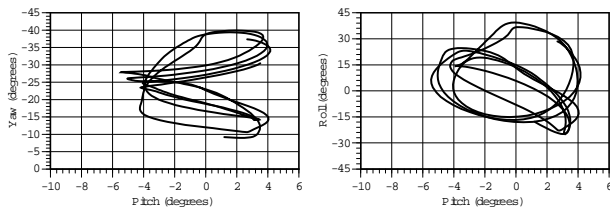

Figure 6. Phase trajectories of sub-harmonic motion obtained from experiment with $H/\lambda = 0.05$, $\lambda/L = 1.25$ and the auto pilot course of -22.5 degrees with $Fn = 0.35$.

From both figures it is found that the period of pitch motion, namely the encounter period approximately, is twice as long as the period of other ship motion mode. Unfortunately because of the limitation on the tank size, longer record is not available, so that it cannot be concluded whether the amplitude of yawing angle becomes larger or not. To specify the relation of the encounter period and the period of other motion modes, we show projections of the trajectories onto pitch-roll and pitch-yaw

planes as Fig.5 and Fig.6. Here a transition to a periodic state is not confirmed in each figure. Comparing the time history and the plot of its projection, it is found that the trajectories tend to double period attractors.

3. MATHEMATICAL MODEL

The mathematical model used in this paper is a manoeuvring model of the surge-sway-yaw-roll motion developed for prediction of broaching associated with surf-riding in following and quartering waves (Umeda, 1999). In cases of ship runs with higher forward velocity in following and quartering waves, the encounter frequency becomes much smaller than the natural frequencies in heave and pitch. Therefore these motions were estimated by simply tracing their stable equilibrium. (Matsuda & Umeda, 1997)
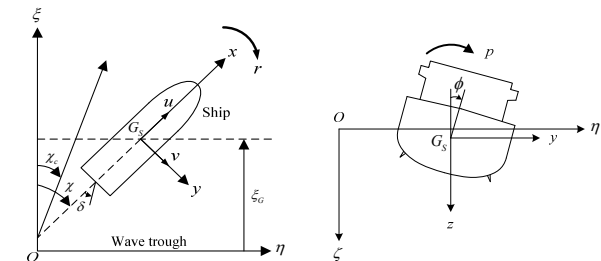

Figure 7. Coordinate systems.

As can be seen in Fig.7, two coordinate systems are used: (1) a wave fixed with its origin at a wave trough, the axis in the direction of wave travel; and (2) an upright body fixed with its origin at the centre of ship gravity, with the x axis pointing toward the bow, the y axis to starboard, and the z axis downward.

Note that henceforth, all vectors are taken as column vectors; a row vector can be obtained from the column vector, and vice versa, by transposition, which is denoted with the *T* superscript. The state vector, **x**, and control vector, **b**, of this system are defined as follows:

$$\mathbf{x} = (x_1, x_2, \cdots, x_8)^T \in \mathbf{R}^8$$
$$\equiv (\xi_G / \lambda, u, v, \chi, r, \phi, p, \delta)^T \quad (1)$$

$$\mathbf{b} \equiv (n, \chi_c)^T \in \mathbf{R}^2 \quad (2)$$

The dynamical system can be represented by the following state equation:

$$\dot{\mathbf{x}} = \mathbf{F}(\mathbf{x}; \mathbf{b}) = [f_1(\mathbf{x}; \mathbf{b}), f_2(\mathbf{x}; \mathbf{b}), \cdots, f_8(\mathbf{x}; \mathbf{b})]^T. \quad (3)$$
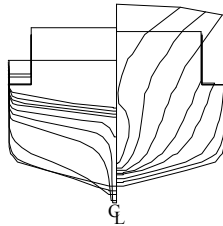
Details of this equation are available in Appendix 1.

Figure 8. Body plan of the subject ship.

Based on the above-mentioned mathematical model, numerical calculations were carried out for a 135GT Japanese purse seiner used in the ITTC benchmark testing (Umeda & Renilson, 2001) whereas the free-running model experiment were carried out using the ONR tumblehome vessel. The principal particulars and body plan are shown in Table 2 and Fig.8, respectively. Hydrodynamic coefficients and other relating parameters can be found in the literature. (Umeda & Hashimoto, 2002)

Table 2. Principal particulars of the ship.

Items	Values
Length: L_{BP}	34.5 m
Breadth: B	7.60 m
Depth: D	3.07 m
Draught at FP: d_f	2.50 m
Mean draught: d_m	2.65 m
Draught at AP: d_a	2.80 m
Block coefficient: C_b	0.597
Metacentric height: GM	1.00 m
Pitch radius of gyration: κ_{yy}/L_{BP}	0.302
L.C.B. (aft)	1.31 m
Rudder Area Ratio	1/26.2
Time constant for steering gear: T_E	0.63 s
Rudder gain: K_P	1.0
Time constant for differential control: T_D	0.0 s

4. PERIODIC SOLUTION

To examine the subharmonic yaw motion, firstly a periodic solution of the system is required. Since the system used here is autonomous, the period should be dealt with as one of unknown parameters. Specifically, setting the section Π which is transverse to periodic solution, we can define Poincaré mapping by which Π maps onto its own (Kawakami et al., 1978). More details of the used method for obtaining a periodic solution of an autonomous system can be found in Appendix 2.

Fig.9 shows the comparison of the above methodology and a simple numerical integration scheme. We can see the asymptotic behaviour of trajectory obtained by numerical integration toward periodic solution. Therefore it can be concluded that numerical accuracy of above calculation scheme is guaranteed.
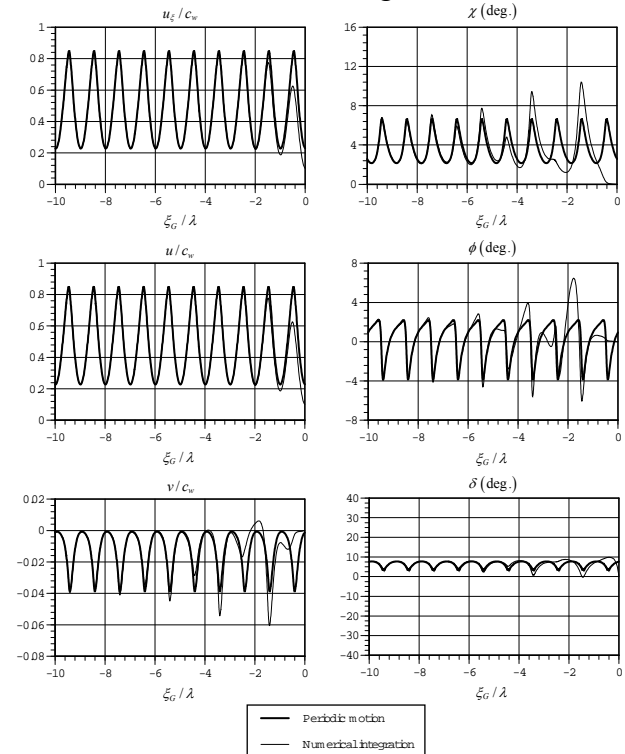

Figure 9. An example of the periodic solution under $H/\lambda = 0.1$, $\lambda/L = 1.637$ and the auto pilot course of 10 degrees with $Fn = 0.3$.

5. FLIP BIFURCATION AND CHAOS

Although the result shown in Fig.9 is a stable periodic solution having period equal to the encounter period, (1T), a periodic solution having different period could appear depending on parameters. As it was mentioned above, period-doubling phenomenon had been first observed by Kan (1982) in model test and further identified by Spyrou (1997) as flip bifurcation. Therefore analysis of eignvalues of a periodic orbit as well as applications of Lyapunov exponent seems to be appropriate here.
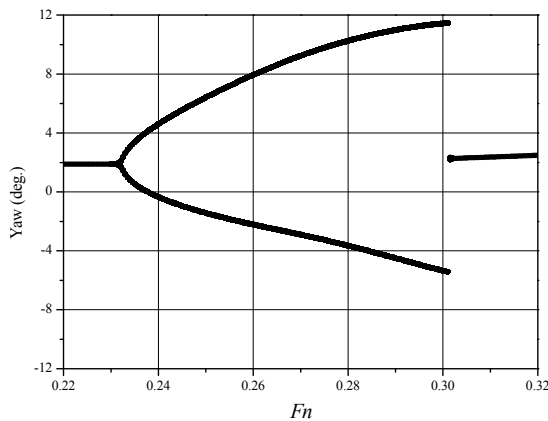

Figure 10. Poincaré mapping versus *Fn* with $H/\lambda = 0.1236$, *λ/L*=1.975 and the auto pilot course of 10 degrees.

Fig.10 shows the Poincaré mapping according to Eq. (B8). As can be seen, trajectory is bifurcated into double period at about $Fn = 0.23$ and returned to 1T periodic solution at about $Fn = 0.3$. And Fig.11 represents one of examples of double period solution (2T) obtained by using above methodology.
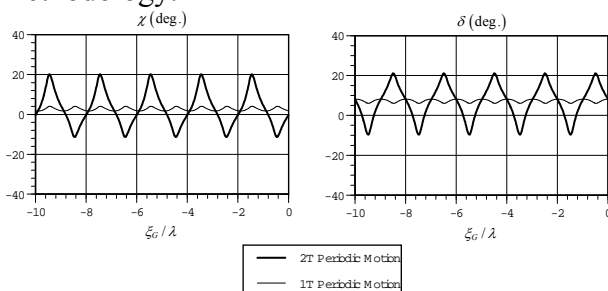

Figure 11. An example of the periodic solution under $H/\lambda = 0.1236$, *λ/L*=1.975 and the auto pilot course of 10 degrees with $Fn = 0.24$.

In this figure though 1T periodic solution is also drawn, taking account of Fig.10, 1T solution must be regarded as unstable. To theoretically demonstrate the stability of periodic solution, i.e. fixed point on Poincaré section, we considered following characteristic polynomial equation;

$$\det[DT(\mathbf{u}_0) - \mu\mathbf{I}] = 0 \qquad (4).$$

Here it is well-known that if this equation has the solution of $\mu = -1$, then the dynamical system has a double period fixed point on Poincaré section.
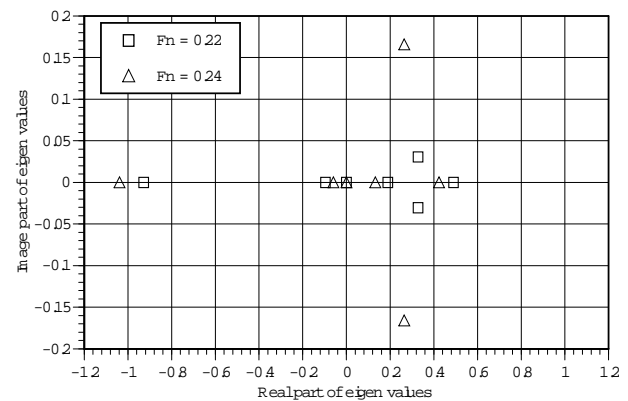

Figure 12. Comparison of the characteristic values as related to Jacobi matrix of Poincaré mapping between *Fn* of 0.22 and 0.24, with $H/\lambda = 0.1236$, *λ/L*=1.975 and the auto pilot course of 10 degrees.

Fig.12 shows the eigenvalue μ of 1T periodic solution, obtained by solving Eq. (4). Here the abscissa represents a real part of eigenvalues whilst the ordinate does an imaginary part of them. From this figure it is found that if the bifurcation of fixed point on Poincaré section happens, eigenvalue crosses the unit circle in complex plane. It clearly demonstrates the flip bifurcation. Likewise, it can be also confirmed that eigenvalue crosses the unit circle in complex plane within *Fn* of 0.29 and 0.30, but it is omitted to plot the figure for the sake of brevity. And although we did not execute further investigation, we can sequentially obtain the parameter which arises flip bifurcation if we solve the Eqs. (B6), (B8) and (4) simultaneously. Then we can

sequentially trace Poincaré map by sweeping parameter (Kawakami & Katsuta, 1981).

It is well-known that sequential flip bifurcations leads to chaotic phenomenon. Fig.13 shows the Poincaré mapping.
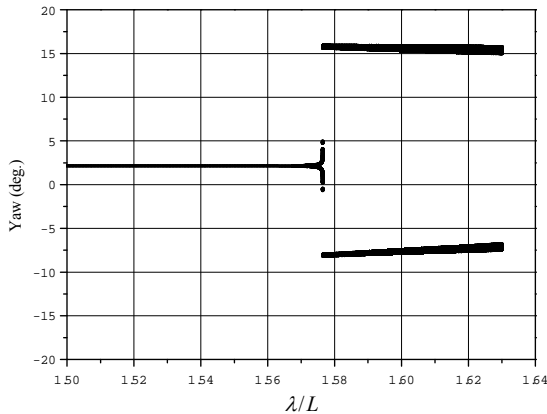

Figure 13. Poincaré mapping versus λ / L with $H / \lambda = 0.1325$, $Fn = 0.28$ and the auto pilot course of 11 degrees.

From this figure it is found that 1T periodic solution becomes unstable at the neighbourhood of $\lambda / L = 1.57$ and then flip bifurcation happens. Fig.14 represents a magnified portrait of the Poincaré section. We can see that as a result of sequential flip bifurcation may lead to the chaotic ship motion.
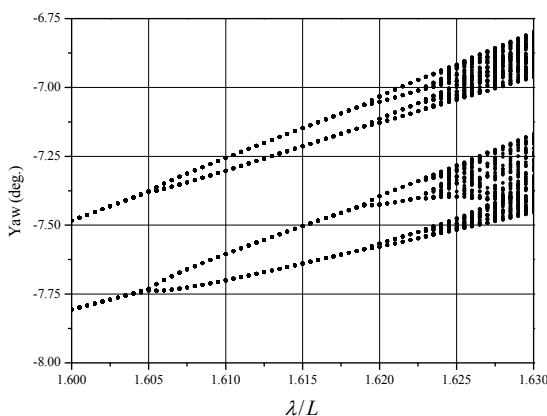

Figure 14. Partially magnified Poincaré mapping versus λ / L with $H / \lambda = 0.1325$, $Fn = 0.28$ and the auto pilot course of 11 degrees.

To quantitatively demonstrate it, we calculated the maximum Lyapunov exponent. Lyapunov exponents describe a way to judge whether nearby trajectories converge or diverge in the state space of a dynamical system by measuring the mean logarithmic growth rate (Geist, K. et al., 1990). If maximum Lyapunov exponent has a positive value, then trajectory has logarithmic instability, i.e. one of characteristics of chaos. Fig.15 indicates the maximum Lyapunov exponent for the same condition to Fig.13.
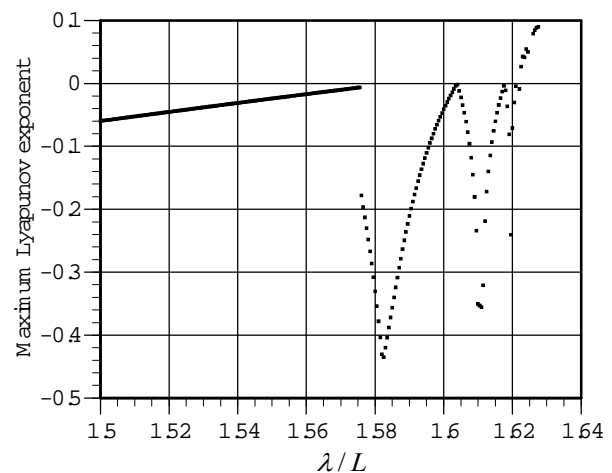
Figure 15. Maximum Lyapunov exponent versus λ / L with $H / \lambda = 0.1325$, $Fn = 0.28$ and the auto pilot course of 11 degrees.

Fig. 15 indicates that the maximum Lyapunov exponent changes its sign from negative to positive at the wavelength to ship length ratio of approximately 1.623. At this condition in Fig. 14 we can notice the limit of sequential flip bifurcation (Feigenbaum cascade). This fact supports that sequential flip bifurcations lead to chaos phenomenon associated with yaw instability.

6. OPTIMAL CONTROL THEORY

Optimal control theory is the theory to obtain the control law realizing the minimum performance index under state equations, constraints and boundary conditions. In our past research (Maki et al., 2008A), utilizing the optimal control theory for ship motion in

following and quartering seas, we obtained the rudder control law which minimizes the course deviation from autopilot course. Numerical calculation technique of optimal control problem can be divided into the two, i.e. the scheme based on variation method and that based on mathematical programming technique. In our past research (Maki et al., 2008B) it was numerically confirmed that the both techniques leads to the same results each other, so that the numerical accuracy is fully guaranteed. Hence in this research we utilized the mathematical programming method as optimization technique. And the optimal periodic solution seems to be powerful aid for the consideration of yaw instability, so that we explain the calculation scheme of it as follows.

First we set the variable $\mathbf{x} \in \mathbf{R}^7$ again as follows;

$$\mathbf{x} \equiv (\xi_G / \lambda, u, v, \chi, r, \phi, p)^T . \qquad (5)$$

Then the optimal control problem in this research to be considered is stated in the following manner: minimize the performance index;

$$J \equiv \frac{1}{t_f} \int_0^{t_f} (\chi - \chi_c)^2 \, dt_f \qquad (6)$$

subject to the differential constraints, i.e. state equation;

$$\dot{\mathbf{x}} = \mathbf{F}(\mathbf{x}, \delta_I, \mathbf{p}; \mathbf{b}) \in \mathbf{R}^7, \qquad (7)$$

the boundary conditions and non-differential constraints;

$$-\delta_{MAX} \le \delta_I(t) \le \delta_{MAX} \quad (0 < t < t_f). \qquad (8)$$

Where $\delta_I(t)$ and $\mathbf{p}$ are the rudder control and the parameter vector, such as final time t_f, respectively. And δ_{MAX} has the value of 35 degrees. In this research we approximately consider that the input rudder angle is just equivalent to actual rudder angle for the sake of brevity, so that the rudder control equation is not taken into account.

As mentioned above, the period of the periodic motion associated with autonomous system is generally axiomatic. Thus the period has to be included among unknown parameters. Here taking the Poincaré section as Eq. (B8), the boundary conditions of optimal periodic solution can be represented as;

$$\mathbf{x}_0 - \mathbf{x}(t_f) = \pm n_T [1, 0, \cdots, 0]^T \in \mathbf{R}^7 . \qquad (9)$$

Here $\mathbf{x}_0$ denotes the boundary state value at one side and integer n_T does period of ship motion.

The optimal control problem stated above is converted to a nonlinear programming problem. To transform the control $\mathbf{u}(t)$ to a set of discrete variables, the time interval $[0, t_f]$ is divided into N segments, being the nodal value of the time is denoted by t_i ($i = 1, 2, \cdots, N+1$). Therefore, control variables can be represented as a set of discrete values $\delta_i = \delta_I(t_i)$. If the initial state values are assumed by boundary condition $\mathbf{x}_0$, and if the control variables $\mathbf{u}_i$ and final time t_f are specified, the state variable can be calculated through the numerical integration scheme. As a result, the nodal values of the states are written as a function with respect to $\mathbf{x}_0$, $\mathbf{u}_i$ ($i = 1, 2, \cdots, N+1$) and t_f. These independent variables are combined into a single vector $\mathbf{X}$ as

$$\mathbf{X} \equiv [\mathbf{x}_0^T, \delta_1, \delta_2, \cdots, \delta_{N+1}, t_f]^T \qquad (10).$$

Then the performance index J and path constrains are function with respect to $\mathbf{X}$. Therefore, the optimal control problem can be formulated in the following nonlinear programming problem:

minimize $J(\mathbf{X})$

subject to $\delta_i^2 - \delta_{MAX}^2 \le 0$ ($i = 1, \cdots, N+1$), (11)

$$\mathbf{x}_0 - \mathbf{x}(t_f) = \pm n_T [1, 0, \cdots, 0]^T$$

where

$$\tilde{J}(\mathbf{X}) \equiv \sum_i \frac{1}{N}[\chi_i(\mathbf{X}) - \chi_c]^2 . \qquad (12)$$

Here the constrains are imposed at each nodal point t_i. Based on the knowledge of mensuration by parts, limitation with respect to N yields following relation;

$$\lim_{N \to \infty} \tilde{J}(\mathbf{X}) = J, \qquad (13)$$

so that Eq. (6) and Eq. (12) are equivalent for large N. Notice that periodic condition to rudder input is not imposed in above formulation. It is because imposing a periodic condition on state value at both ends simultaneously imposes a periodic condition on rudder input. It can be mathematically proved. Its proof and detailed explanation about it are omitted for the sake of brevity, but it will be published in a separate paper.

In this research the numerical optimization using mathematical programming is carried out utilizing programming package of sequential quadratic programming (SQP) method. And the derivatives of performance index are calculated by using numerical differentiation whereas it can be obtained introducing sensitivity differential equation (Tsuchiya & Suzuki, 1997).

7. APPLICATION OF OPTIMAL CONTROL THEORY

As it was shown by Spyrou (1997) the rational choice of differential gain may decrease or even completely exclude yaw instability. Therefore choice of the autopilot gains becomes a safety factor. Here an attempt is made to use optical control theory for this choice. Not arguing on importance of differential control, the authors have chosen to focus on proportional control only as the first step.

Following above formulation, we executed the numerical optimisations. Fig.16 shows the comparison of the periodic solutions obtained

by two different proportional controls and optimal control. For this wave condition large-amplitude subharmonic yaw motion is realised with proportional gain of 2.0 whereas it is not done with proportional gain of 1.0. This result corresponds with that shown by Spyrou (1997) and Umeda et al. (2008B). In the case of proportional gain of 1.0, although amplitude of yaw motion is small, mean of yaw angle is deviated from desired course due to wave-induced yaw moment. Hence it is concluded that the course-keeping of both proportional controls has more or less problematic aspect. On the other hand, obtained optimal rudder control successfully keeps her desired course with relatively small amplitude of yaw motion as a Bang-Bang control. Here the state equation and performance index which we use in this research have linear relation with respect to rudder input, so that it can be proved for such system that optimal rudder input generally becomes Bang-Bang type except for quite special case (Maki et al., 2008C). Base on this knowledge it is found that the accuracy of numerical calculation is fully ensured.

Figure 16. Comparison of rudder and yaw angles as a function of longitudinal ship position between the optimal control and two different proportional controls with $\lambda / L = 1.975$, $H / \lambda = 0.1236$, $Fn = 0.206$ and the auto pilot course of 10 degrees.

Fig.17 shows the numerical results with the condition which leads to the chaotic ship motion.

Since a periodic solution does not exist with the condition which leads to the chaotic

oscillation, trajectory with proportional control is obtained using simple numerical integration.
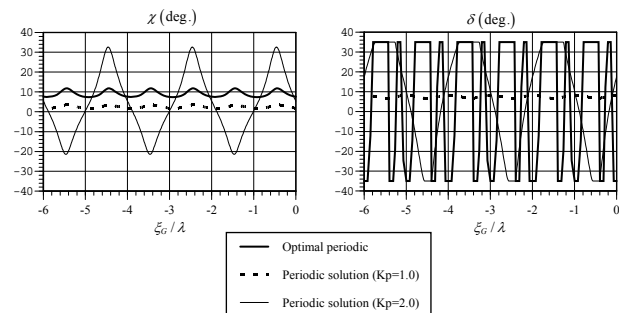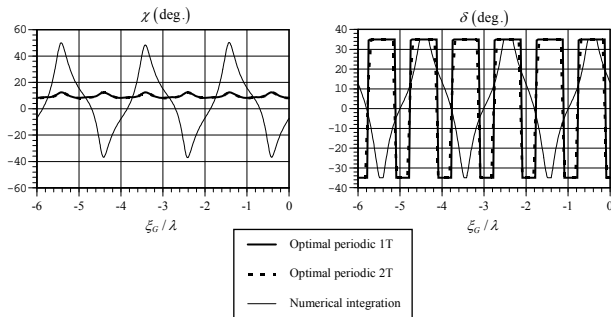

Figure 17. Comparison of rudder and yaw angles as a function of longitudinal ship position between the optimal control and the proportional controls which have different period each other, with $\lambda / L = 1.6275$, $H / \lambda = 0.1325$, $Fn = 0.28$ and the auto pilot course of 10 degrees.

From this figure it is founded that large-amplitude subharmonic yaw motion can be completely prevented utilizing the optimal rudder control as Bang-Bang control with the condition which arises not only subharmonic yaw motion but also chaotic ship motion. Furthermore optimal 2T trajectory is plotted in this figure. However since its tendency completely coincides with the result of 1T optimal control, it is concluded that an optimal 2T periodic solution does not locally exist. Nonetheless, we cannot reject the possibility of existence of the global optimal 2T solution. To realize such global optimal solution, generic algorithm (GA) (Goldberg, 1989) is applicable. It is our future task.

As mentioned above, it is revealed that subhatrmonic yaw motion can be prevented by appropriate rudder control, so that this knowledge could facilitate to the development of autopilot and operational guidance for preventing this phenomenon. And validation of obtained result through free-running model experiment is desirable.

8. CONCLUDING REMARKS

Experimental records of subharmonic yaw motion were successfully obtained. Then a standard bifurcation technique of periodic orbits confirmed that the occurrence of this phenomenon can be regarded as a flip bifurcation. The calculation of Lyapunov exponents indicates that this phenomenon could result in chaos. Furthermore obtained optimal rudder control successfully prevents the occurrence of the subharmonic yaw motion whilst the proportional autopilot does not. This suggests, if this conclusion is widely applicable for ships, that this oscillatory broaching could be avoided by appropriate operation. Therefore, oscillatory yaw instability could be noted in physics-based operational guidance but it does not have to be included in a design criterion.

9. ACKNOWLEDGEMENTS

10. APPENDIX 1

Following equations represent the each component of state equations used in this research.

$$f_1(\mathbf{x};\mathbf{b}) = (u\cos\chi - v\sin\chi - c)/\lambda \qquad (A1)$$

$$f_2(\mathbf{x};\mathbf{b}) = [T(u;n) - R(u) + X_w(\xi_G/\lambda,\chi)] \\ /(m+m_x) \qquad (A2)$$

$$f_3(\mathbf{x};\mathbf{b}) = [-(m+m_x)ur + Y_v(u;n)v + Y_r(u;n)r \\ + Y_\phi(u)\phi + Y_\delta(u;n)\delta \\ Y_w(\xi_G/\lambda,u,\chi;n)]/(m+m_y) \qquad (A3)$$

$$f_4(\mathbf{x};\mathbf{b}) = r \qquad (A4)$$

$$f_5(\mathbf{x};\mathbf{b}) = [N_v(u;n)v + N_r(u;n)r + N_\phi(u)\phi$$
$$+ N_\delta(u;n)\delta + N_w(\xi_G/\lambda,u,\chi;n)] \quad \text{(A5)}$$
$$/(I_{ZZ} + J_{ZZ})$$

$$f_6(\mathbf{x};\mathbf{b}) = p \quad \text{(A6)}$$

$$f_7(\mathbf{x};\mathbf{b}) = [m_x z_H u r + K_v(u;n)v + K_r(u;n)r$$
$$+ K_P(u)p + K_\phi(u)\phi + K_\delta(u;n)\delta$$
$$+ K_w(\xi_G/\lambda,u,\chi;n) + mgGZ(\phi)] \quad \text{(A7)}$$
$$/(I_{xx} + J_{xx})$$

$$f_8(\mathbf{x};\mathbf{b}) = [-\delta - K_R(\chi - \chi_C) - K_R T_D r]/T_E \quad \text{(A8)}$$

11. APPENDIX 2

In the following we describe this scheme and calculate a periodic attractor. Let a solution of Eq. (3), i.e. the trajectory, as the following form;

$$\mathbf{x}(t) = \text{ш}(t;t_0,\mathbf{x}_0) \in \mathbf{R}^8 \quad \text{(B1)}$$

Here we take a local cross section Π;

$$\Pi = \{\mathbf{x} \in \mathbf{R}^8 | g(\mathbf{x}) = 0, g : \mathbf{R}^8 \to \mathbf{R}\} \quad \text{(B2)}.$$

Where $g(\mathbf{x}) = 0$ represents the 7-dimensional hypersurface describing the Poincaré section Π. The hyper surface Π need not be planer, but must be chosen so that the flow is everywhere transverse to it. And set a local ordinate;

$$h : \Pi \to \Sigma \subset \mathbf{R}^7 \quad \text{(B3)}.$$

Denote the points where trajectory transversally intersects Σ by;

$$\mathbf{x}_0, \mathbf{x}_1, \cdots$$

and define its Poincaré mapping onto Σ;

$$h(\mathbf{x}_0) = \mathbf{u}_0, h(\mathbf{x}_1) = \mathbf{u}_1, \cdots$$

Let the trajectory which has the initial value $h^{-1}(\mathbf{u}_0) = \mathbf{x}_0$ at $t = t_0$ intersects Π at $\mathbf{x}_1$ and let its time $t = t_0 + \tau(\mathbf{x}_0)$, as follows;

$$\mathbf{x}_1(t) = \text{ш}(t_0 + \tau(h^{-1}(\mathbf{u}_0)); t_0, \mathbf{x}_0). \quad \text{(B4)}$$

Here we take the map T by which Σ maps onto its own as follows;

$$T : \Sigma \to \Sigma ; \mathbf{u}_0 \mapsto \mathbf{u}_1$$
$$= h(\text{ш}(t_0 + \tau(h^{-1}(\mathbf{u}_0)); t_0, h^{-1}(\mathbf{u}_0))) \quad \text{(B5)}$$

Then a periodic solution must satisfy following relation;

$$T(\mathbf{u}_0) = \mathbf{u}_0. \quad \text{(B6)}$$

And also following relation must be satisfied;

$$g(\mathbf{x}) = 0 \quad \text{(B7)}$$

Hence it is required to simultaneously solve Eq. (17) and Eq. (18) with respect to $\mathbf{u}_0$ and τ by Newton method. In this research we take Poincaré section as;

$$g(\mathbf{x}) \equiv \xi_G/\lambda - [\xi_G/\lambda] - \nu \quad \text{(B8)}$$

Here ν represents the constant within the set of $[0,1)$, and $[\cdots]$ means floor function. In this paper we set ν of zero and all the derivatives existed in Newton iteration was obtained using numerical differentiation.

12. REFERENCES

Geist, K., Parlitz, U. and Lauteborn, W., 1990, "Comparison of Different Methods for Computing Lyapunov Exponents", Progress of Theoretical Physics, Vol.83, No.5, pp.875-893.

Goldberg, D.E., 1989, Generic Algorithm in Search, Optimization & Machine Learning, Addison Wesley.

Japan, the Netherlands and the United States, 2007, Framework for the Development of New Generation Criteria for Intact Stability, SLF 50/4/4, IMO (London), pp.1-6.

Kan, M., Saruta, T., Taguchi, H. Et al., 1990, "Capsizing of a Ship in Quartering Seas (Part 1)" Journal of the Society of Naval Architects of Japan, Vol.167, pp.81-90 (in

Japanese).

Kawakami, H., Matsumura, T. and Kobayashi, K., 1978, "An Algorithm to Obtain the Periodic Solutions on Autonomous Systems", The Transactions of the Institute of Electronics and Communication Engineers of Japan, J61-A, No.10, pp.1051-1053, (in Japanese).

Kawakami, H. and Katsuta, Y., 1981, "The Hopf Bifurcation and Chaos States of Solutions in a Third Order Equation of Duffing's Type", The Transactions of the Institute of Electronics and Communication Engineers of Japan, J64-A, No.11, pp.940-947, (in Japanese).

Maki, A., Umeda, N. and Ueno, S., 2008A, "Application of Optimal Control Theory to Course Keeping Problem in Following Seas", Journal of the Japan Society of Naval Architects and Ocean Engineers, Vol.7, pp.207-212, (in Japanese).

Maki, A., Umeda, N. and Ueno, S., 2008B, "Investigation on Broaching-to Using Optimal Control Theory", Journal of the Japan Society of Naval Architects and Ocean Engineers, Vol.8, pp.115-122, (in Japanese).

Maki, A., Umeda, N. and Ueno, S., 2008C, "Effect of Wave-induced Periodic Forces on Optimal Course Control of a Ship", Proceedings of 25th SICE Symposium on Guidance and Control, pp.103-109, (in Japanese).

Matsuda, A. and Umeda, N., 1997, "Vertical Motions of a Ship Running in Following and Quartering Seas" Journal of the Kansai Society of Naval Architects, Vol.227, pp.47-55 (in Japanese).

Motora, S., Fujino, M. and Fuwa, T., 1982, "On the Mechanism of Broaching-To Phenomena", Proceedings of the 2nd International Conference on Stability and Ocean Vehicles, Tokyo, pp.535-550.

Oakley, O.H,, Paulling, J.R. and Wood, P.D., 1974, "Ship Motions and Capsizing in Astern Seas", Proceedings of the 10th Naval Hydrodynamics Symposium, MIT, 1V-1, pp.1-51.

Spyrou, K.J., 1996, "Dynamic Instability in Quartering Seas-Part II: Analysis of Ship Roll and Capsize for Broaching", Journal of Ship Research, Vol. 40, No 4, pp. 326-336.

Spyrou, K.J., 1997, "Dynamical Instability in Quartering Seas-Part III: Nonlinear Effects on Periodic Motions", Journal of Ship Research, Vol. 41, No.3, pp. 210-223.

Tsuchiya, T. and Suzuki, S., 1997, "Computational Method of Optimal Control Problem Using Mathematical Programming (1st Report) Introduction of Sensitivity Differential Equations", Transactions of the Japan Society for Aeronautical and Space Science, Vol.54, No.519, pp.37-43.

Umeda, N. and Renilson, M.R., 1994, "Broaching of a Fishing Vessel in Following and Quartering Seas", Proceedings of the 5th International Conference on Stability of Ships and Ocean Vehicles, Florida Institute, Vol.3, pp.115-132.

Umeda, N., 1999, "Nonlinear Dynamics on Ship Capsizing due to Broaching in Following and Quartering Seas", Journal of Marine Science of Technology, Vol.4, pp.16-26.

Umeda, N., Matsuda, A., Hamamoto, M. and Suzuki, S., 1999, "Stability Assessment for Intact Ships in the Light of Model Experiments", Journal of Marine Science of Technology, Vol.4, pp.45-57.

Umeda, N. and Renilson, M.R., 2001, "Benchmark Testing of Numerical Prediction on Capsizing of Intact Ships in Following and Quartering Seas", Proceedings of the 5th International Workshop on Stability and Operational

Safety of Ships, University of Trieste, pp.6.1.1-10.

Umeda, N. and Hashimoto, 2002, "Qualitative Aspects of Nonlinear Ship Motions in Following and Quartering Seas with High Forward Velocity", Journal of Marine Science and Technology, Vol., 6, pp. 111-121.

Umeda, N., Yamamura, S., Matsuda, A., Maki, A. and Hashimoto, H., 2008A, "Model Experiments on Extreme Motions of a Wave-Piercing Tumblehome Vessel in Following and Quartering Waves", Journal of the Japan Society of Naval Architects and Ocean Engineers, Vol.8, pp.123-129.

Umeda, N., Araki, M. and Hashimoto, H., 2008B, "Numerical Simulation on Dynamic Behaviour of a Trimaran Running in Following and Quartering Waves", Proceedings of 3rd PAAMES and AMEC2008, Makuhari, pp.197-203, 2008B.

13. NOMENCLATURE

c wave celerity
Fn nominal Froude number
g gravitational acceleration
GZ righting arm
H wave height
I_{xx} moment of inertia in roll
I_{zz} moment of inertia in yaw
J_{xx} added moment of inertia in roll
J_{zz} added moment of inertia in yaw
K_p derivative of roll moment with respect to roll rate
K_P rudder gain
K_r derivative of roll moment with respect to yaw rate
K_T thrust coefficient of propeller
K_v derivative of roll moment with respect to sway velocity
K_w wave-induced roll moment

K_δ derivative of roll moment with respect to rudder angle
K_ϕ derivative of roll moment with respect to roll angle
L ship length between perpendiculars
m ship mass
m_x added mass in surge
m_y added mass in sway
n propeller revolution number
N_r derivative of yaw moment with respect to yaw rate
N_v derivative of yaw moment with respect to sway velocity
N_w wave-induced yaw rate
N_δ derivative of yaw moment with respect to rudder angle
N_ϕ derivative of yaw moment with respect to roll angle
p roll rate
r yaw rate
R ship resistance
t time
T propeller thrust
T_D time constant for differential control
T_E time constant for steering gear
u surge velocity
v sway velocity
X_w wave-induced surge force
Y_r derivative of sway force with respect to yaw rate
Y_v derivative of sway force with respect to sway velocity
Y_w wave-induced sway force
Y_δ derivative of sway force with respect to rudder angle
Y_ϕ derivative of sway force with respect to roll angle
z_H vertical position of centre of sway force due to lateral motions
δ rudder angle
λ wave length
ξ_G longitudinal position of centre of gravity
ϕ roll angle
χ heading angle from wave direction
χ_c desired heading angle for auto pilot